An Adaptive Single-phase Reclosing Technique for Wind Farm Transmission Lines Based on SOD Transformation of CVT Secondary Voltage

Hongchun Shu, Cong Li, Yue Dai, Yutao Tang, and Yiming Han

***Abstract*—Automatic reclosing is widely employed in wind farm transmission lines. However, conventional reclosing strategies cannot identify the nature of the fault before reclosing, thereby posing a risk to the safe operation of the wind farm transmission system and associated equipment, especially during permanent faults. This study focuses on 220 kV wind farm transmission lines without parallel reactors. A single-phase ground fault circuit model is established first, and expressions for faulted phase-end voltages are derived before and after arc extinction. Then, the variations in voltage amplitude before and after fault arc extinction are revealed. The short-time Fourier transform is employed to extract fundamental frequency voltage amplitude from the secondary side of the capacitive voltage transformer (CVT). Subsequently, an adaptive reclosing strategy based on fundamental frequency voltage amplitude detection for wind farm transmission lines is proposed to enhance feature variations through sequential overlapping derivative (SOD) transformation. Finally, through analysis and validation on the RTDS platform, the proposed adaptive reclosing strategy is demonstrated to be simple, feasible, robust against transient resistances, and characterized by high sensitivity.**

***Index Terms*—Adaptive reclosing, CVT, fault nature, SOD, wind farm transmission lines.**

I. Introduction

In recent years, wind power generation has rapidly gained prominence due to its pollution-free nature, low operational costs, and widespread availability [1]. However, the operational conditions of wind farm transmission systems often encounter adverse weather conditions, resulting in a heightened probability of system faults [2]. Statistics indicate that small to medium-sized wind farms generally connect to the grid through overhead transmission lines at 110 kV or 220 kV [3]. Moreover, transient single-phase faults constitute most overhead transmission line faults. Reclosing breakers can effectively restore the power supply if these transient faults disappear, and therefore, reclosing device installation can ensure continuous and stable outward transmission of electrical energy from wind farms. Currently, reclosing devices installed in transmission lines within wind farms typically employ traditional reclosing strategies, involving indiscriminate reclosing after a fixed delay irrespective of whether a fault-triggered breaker trip is due to a transient or permanent fault on the transmission lines. If reclosing occurs during a permanent fault or before the extinction of the secondary arc, reclosing may fail, causing secondary impacts on the system and affecting its stability. To address this, accurately identifying the nature of the fault before reclosing and executing specific reclosing strategies based on the identified results hold paramount significance for the reliable operation of wind farm transmission systems and the safety and stability of electrical equipment.

Recently, numerous scholars have conducted extensive research on the reclosing technology of wind farm transmission lines. Reference [4] analyzes the reasons behind wind farm islanding caused by automatic reclosing on permanent faults, and proposes to prolong reclosing initiation time to decrease secondary drop current by altering the reclosing functional configuration. References [5]–[7] present the low success rate of reclosing on the wind farm side using the "check synchronous" method and suggest alternative reclosing methods, such as "check busbar no voltage line has voltage" and "continuously check busbar no voltage" to enhance reclosing success rates. However, these reclosing schemes mainly focus on the success of reclosing initiation while overlook secondary impacts on the wind farm transmission system due to reclosing on permanent faults. Reference [8] introduces an adaptive reclosing strategy based on the active-to-reactive power

Received: August 25, 2024
Accepted: March 3, 2025
Published Online: July 1, 2025
Hongchun Shu, Cong Li, Yue Dai (corresponding author), Yutao Tang, and Yiming Han are with the Yunnan Key Laboratory of Green Energy, Electric Power Measurement Digitalization, Control and Protection, Kunming University of Science and Technology, Kunming 650500, China (e-mail: shuhongchun@kust.edu.cn; 13531037695@163.com; 1769624266@qq.com; kusttyt@sina.cn; 373482753@qq.com).
DOI: 10.23919/PCMP.2024.000162

ratio on the faulty phase of wind farm transmission lines. However, this method requires to extract multiple frequency components from the faulty phase power, complicating filtering processes. Reference [9] developes a phase-separated reclosing strategy targeting different natures of faults on wind farm transmission lines by initially reclosing specific phases and using inter-phase coupled voltage to identify the nature of the fault. However, the accuracy of the fault phase selection can significantly influence the effectiveness of this reclosing strategy. In [10], an active detection-based adaptive reclosing for transmission lines is proposed by injecting low current into the line and using the integrated amplitude of the injected current for fault nature identification. However, this approach cannot detect single-phase ground faults in non-injected phases and requires multiple injections of signals. Reference [11] presents a method for calculating the reclosing time of wind farm transmission lines based on the changing process of wind turbine stator voltage in different stages after a transient fault. However, the paper does not provide a methodology for setting the stator voltage threshold. The abovementioned studies provid various advantageous insights into adaptive reclosing technology, serving as a valuable reference and inspiration for future researchers. Nevertheless, the proposed solutions face limitations in real-time fault disappearance detection with added complexity of equipment installation for reclosing operations. Hence, this paper presents a single-phase adaptive reclosing technique for wind farm transmission lines based on sequential overlapping derivative (SOD) transformation of the capacitive voltage transformer (CVT) secondary voltage.

This study delves into wind farm transmission lines without parallel reactors by analyzing their operational characteristics during single-phase ground faults and deriving the voltage expression for the faulty phase post-circuit breaker tripping. Employing short-time Fourier transform (STFT) to capture the fundamental frequency voltage amplitude of the faulty phase from the CVT secondary side, SOD transformation is applied for cyclic detection. Real-time fault nature discrimination relies on whether the detection value surpasses the preset threshold. The fault duration is calculated utilizing the detection results, and a single-phase adaptive reclosing strategy tailored for wind farm transmission lines is proposed. A transmission lines model for the wind farm is constructed on the RTDS platform for fault testing, while results are compared with traditional automatic reclosing strategies and existing adaptive reclosing strategies to validate the feasibility of the proposed reclosing scheme.

The remainder of this paper is organized as follows. Section II presents the analysis of single-phase ground fault phase terminal voltage characteristics. Section III introduces the STFT and SOD algorithms. Section IV proposes the single-phase adaptive reclosure strategy. Section V verifies the feasibility of the single-phase adaptive reclosure strategy proposed in this paper through the RTDS platform, and Section VI presents the main conclusions of the paper.

II. Analysis of Single-phase Ground Fault Phase Terminal Voltage Characteristics

The topology of a 220 kV wind farm transmission system is illustrated in Fig. 1, where 100 double-fed induction generator (DFIG) units are installed. The wind farm's box transformers adopt a Ynd connection, and the main transformer adopts a Dyn connection. The distance of the wind farm transmission line is 100 km. When a single-phase ground fault occurs on the transmission lines, protective actions disconnect the faulty phase, leading to non-full-phase operation. Due to the coupling effect between the healthy and the faulty phases, the voltage on the faulty phase is non-zero. Moreover, distinctions exist in the voltage on the faulty phase for different fault natures. The following analysis focuses on the coupled voltage on the faulty phase when different single-phase faults occur on the lines.

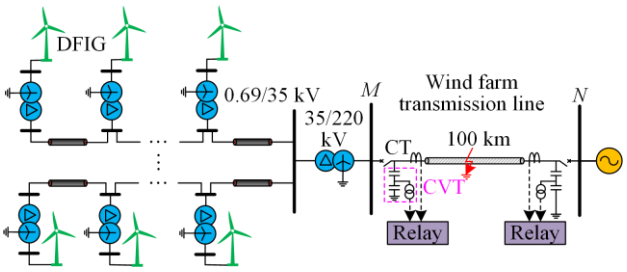

Fig. 1. Topology of 220 kV wind farm transmission system.

A. Analysis of Terminal Voltage Characteristics During a Transient Fault Phase

For convenience in analysis, the system is commonly divided into four stages during a transient single-phase fault on the transmission lines: the pre-fault normal operation stage, the first arc stage, the second arc stage, and the recovery voltage stage [12]. Schematic diagrams representing different stages of transient single-phase ground faults are illustrated in Fig. 2.

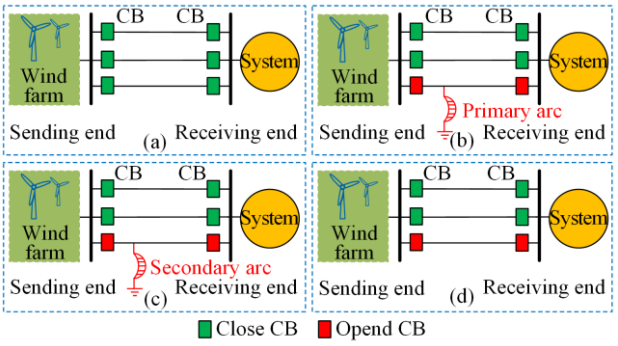

Fig. 2. Schematic diagrams of different stages in transient single-phase ground faults. (a) Normal operation stage. (b) Primary arc stage. (c) Secondary arc stage. (d) Recovery voltage stage.

Figure 2(a) illustrates the schematic diagram of the transmission lines under normal operating conditions, where the wind farm transmission system maintains a stable equilibrium during normal operation. Figure 2(b) depicts the schematic diagram during the primary arc stage. At this stage, the transmission lines experience a transient single-phase ground fault, where the circuit breaker remains closed, and the faulty phase continues to be energized by the system. Figure 2(c) represents the schematic diagram during the secondary arc stage, where the circuit breakers on both side of the faulty phase trip, discontinuing the continuous power supply from the system and placing the wind farm transmission system into a state of partial phase operation. Figure 2(d) portrays the schematic diagram during the recovery voltage stage. When the secondary arc is extinguished, the voltage across the faulty phase primarily consists of the induced voltage between the healthy and faulty phases [13].

This study employs a control theory model to simulate the arc process while disregarding line impedance to analyze the characteristics of fault phase arc voltage. During the secondary arc stage, the fault phase voltage mostly comprises two components: electromagnetic coupling voltage and capacitive coupling voltage. The electromagnetic coupling voltage is induced by the electromagnetic coupling when the current flows through the open fault phase from the healthy phase. Its value is primarily determined by the current in the healthy phase and the mutual inductance impedance between the healthy and faulty phases. The expression for the electromagnetic coupling voltage is as follows:

$$U_{\mathrm{x}} = (I_{\mathrm{B}} + I_{\mathrm{C}}) Z_{\mathrm{m}} l \tag{1}$$

where I_{B} and I_{C} denote the currents of the healthy B-phase and C-phase, respectively; Z_{m} indicates the per-unit line length mutual impedance; and l represents the length from the measuring end to the fault location.

Upon the tripping of the faulted phase, the healthy phase currents (I_{B} and I_{C}) experience minimal changes during both the second arc and recovery voltage stages. Additionally, the per-unit line length mutual inductance, Z_{m} , and line length, l, remain constant. Consequently, the electromagnetically coupled voltages of the faulted phase exhibit negligible differences in these two stages. Therefore, the analysis of the voltage variations in the faulted phase can be effectively approached by examining the capacitive coupled voltage. The magnitude of the capacitive coupled voltage is determined by the ground capacitance and phase-to-phase capacitance of the transmission lines. Upon the occurrence of a transient fault and subsequent tripping of the faulted phase, the equivalent circuit of the lines is depicted in Fig. 3(a).

The circuit for calculating the capacitive coupling component of the secondary arc is illustrated in Fig. 3(b). The frequency domain expression for the fault-phase terminal voltage $U_{\mathrm{a}}(s)$ can be obtained by employing operational methods for solving:

$$U_{\mathrm{a}}(s) = \frac{\dfrac{R_{\mathrm{arc}}/(C_0 s)}{R_{\mathrm{arc}} + 1/(C_0 s)}}{\dfrac{R_{\mathrm{arc}}/(C_0 s)}{R_{\mathrm{arc}} + 1/(C_0 s)} + 1/(2C_{\mathrm{m}} s)} \frac{U_{\mathrm{B}} + U_{\mathrm{C}}}{2}(s) \tag{2}$$

where R_{arc} represents the resistance of the secondary arc; C_0 denotes the capacitive coupling to ground; and C_{m} indicates the interphase capacitive coupling; in addition, U_{B} and U_{C} stand for the non-fault B and C phase voltages, respectively.

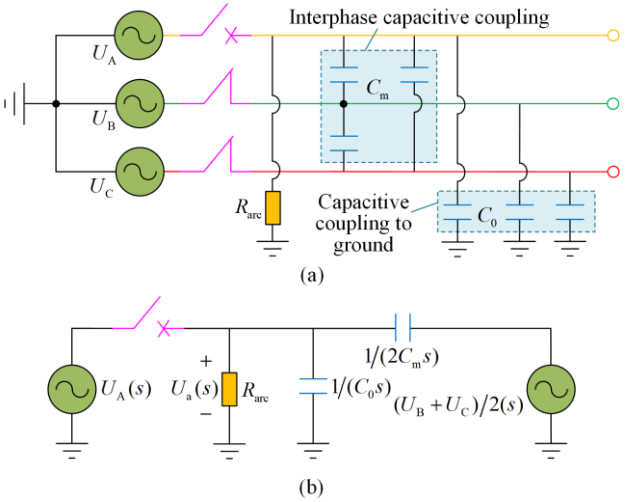

Fig. 3. Circuit diagram of secondary arc stage. (a) Equivalent circuit. (b) Computational circuit.

After the disconnection of the faulted phase, according to [14], the resistance of the secondary arc is far lower than the parallel capacitance impedance of the line. Moreover, the following relationship exists:

$$\begin{cases} R_{\mathrm{arc}} = \dfrac{1}{C_0 s} \\ R_{\mathrm{arc}} = \dfrac{1}{2C_{\mathrm{m}} s} \end{cases} \tag{3}$$

According to (3), equation (2) can be simplified as:

$$U_{\mathrm{a}}(s) = 2C_{\mathrm{m}} s R_{\mathrm{arc}} \frac{U_{\mathrm{B}} + U_{\mathrm{C}}}{2}(s) \tag{4}$$

Its time domain expression can be derived by inverse Laplace transform as follows:

$$U_{\mathrm{a}}(t) = C_{\mathrm{m}} R_{\mathrm{arc}} \frac{\mathrm{d}\left(U_{\mathrm{B}}(t) + U_{\mathrm{C}}(t)\right)}{\mathrm{d}t} \tag{5}$$

When a transient single-phase fault occurs, and after the secondary arc is extinguished, the system transitions into the voltage recovery stage, depicted by its equivalent circuit in Fig. 4(a). The fault grounding arc resistance disappears at this point, effectively rendering R_{arc} infinite. Figure 4(b) represents the equivalent cir-

cuit for the capacitive coupling component, and the faulted phase terminal voltage can be expressed as:

$$U_{\mathrm{a}}(s)=\frac{2C_{\mathrm{m}}s}{C_0 s+2C_{\mathrm{m}}s}\times\frac{U_{\mathrm{B}}+U_{\mathrm{C}}}{2}(s) \tag{6}$$

Its time domain expression can be derived by inverse Laplace transform as follows:

$$U_{\mathrm{a}}(t)=\frac{C_{\mathrm{m}}}{C_0+2C_{\mathrm{m}}}\times\left[U_{\mathrm{B}}(t)+U_{\mathrm{C}}(t)\right] \tag{7}$$

The ratio of (4) to (6) is defined as K to compare the relationship between the faulted phase voltage before and after the fault disappearance, yielding the following relationship:

$$K=\frac{2R_{\mathrm{arc}}C_{\mathrm{m}}s\times\dfrac{U_{\mathrm{B}}+U_{\mathrm{C}}}{2}(s)}{\dfrac{2C_{\mathrm{m}}s}{C_0 s+2C_{\mathrm{m}}s}\times\dfrac{U_{\mathrm{B}}+U_{\mathrm{C}}}{2}(s)}=R_{\mathrm{arc}}(C_0 s+2C_{\mathrm{m}}s) \tag{8}$$

According to (3), with $R_{\mathrm{arc}}C_0 s\ll 1$ and $2R_{\mathrm{arc}}C_{\mathrm{m}}s\ll 1$, substituting into (8) yields $K\ll 1$. The value of K indicates that the faulted phase voltage will significantly increase after the secondary arc is extinguished and the system enters the recovery voltage stage. This phenomenon provides a basis for the subsequent identification of fault nature.

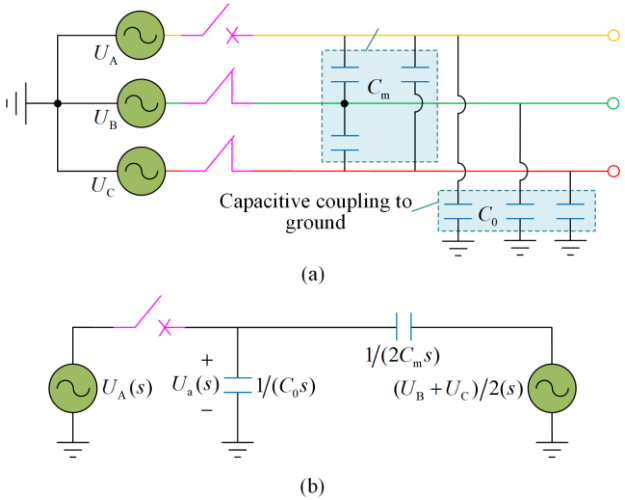

Fig. 4. Circuit diagram of recovery voltage stage. (a) Equivalent circuit. (b) Computational circuit.

B. Analysis of Permanent Fault Phase Terminal Voltage Characteristics

When a permanent single-phase ground fault occurs on the transmission lines, its equivalent circuit matches that shown in Fig. 3 after the circuit breaker trips. According to (4), the frequency domain expression of the faulty-phase terminal voltage $U_{\mathrm{a}}(s)$ is obtained using operational methods:

$$U_{\mathrm{a}}(s)=2C_{\mathrm{m}}sR_{\mathrm{g}}\frac{U_{\mathrm{B}}+U_{\mathrm{C}}}{2}(s) \tag{9}$$

where R_{g} represents the transition resistance.

Its time domain expression can be derived by inverse Laplace transform as follows:

$$U_{\mathrm{a}}(t)=C_{\mathrm{m}}R_{\mathrm{g}}\frac{\mathrm{d}\left(U_{\mathrm{B}}(t)+U_{\mathrm{C}}(t)\right)}{\mathrm{d}t} \tag{10}$$

According to the above analysis, during a transient single-phase fault in wind farm transmission lines, the faulted phase voltage magnitude significantly increases upon extinguishing the secondary arc and entering the recovery voltage stage. However, in the case of a permanent single-phase fault in the wind farm transmission lines, no significant change is observed in the faulted phase voltage after the circuit breaker trips.

Furthermore, whether a transient fault or a permanent fault occurs on the transmission lines, when the circuit breaker trips and enters a non-full-phase operation state, the coupling voltage on the faulted phase mainly consists of the fundamental frequency component during the secondary arc and recovery voltage stages because both the electromagnetic coupling voltage and the capacitive coupling voltage on the faulted phase are coupled from the healthy phase [15]. Therefore, the faulted phase voltage magnitude at power frequency can be utilized to identify fault nature.

III. Extraction and Enhancement of Power Frequency Components

A. STFT

The fault voltage signal is non-stationary, and the Fourier transform can only provide the global frequency spectrum information and cannot reveal the moments when each frequency component appears. Moreover, the Fourier transform struggles to promptly capture signal mutations. STFT effectively resolves these challenges by addressing the issues mentioned above. The STFT of $x(t)$ is mathematically defined as follows [16]:

$$F_{\mathrm{STFT}x}(t,f)=\int_{-\infty}^{\infty}x(u)g^{*}(u-t)\mathrm{e}^{-\mathrm{j}2\pi fu}\mathrm{d}u \tag{11}$$

where f represents the frequency variable; u represents the integral variable; and $g^{*}(\cdot)$ represents the time window function.

For a given time t, $F_{\mathrm{STFT}x}(t,f)$ can be considered as the spectrum at that moment. However, it is necessary to discretize $F_{\mathrm{STFT}x}(t,f)$ in practical applications. Sampling the signal $x(k)$ at regular intervals in the time-frequency domain with (mT, nF), where T represents the time domain sampling period; F indicates the frequency domain sampling period; and k, m, $n=0,1,\cdots,N-1$, with N being the total number of sampling points, the STFT of $x(k)$ is defined as follows:

$$F_{\mathrm{STFT}x}(m,n)=\sum_{0}^{N-1}x(k)g^{*}(k-m)\mathrm{e}^{-\mathrm{j}2\pi nk/N} \tag{12}$$

This paper applies STFT to the raw voltage signal to precisely capture voltage amplitude variations at power

frequency. This step is crucial for subsequent analysis of fault nature.

B. SOD Transformation

This paper proposes an algorithm based on SOD transformation to further enhance the amplitude variation characteristics of the voltage signal at power frequency and improve discrimination. The SOD transformation is a differential operation-based method, involving multiple-order differences, where the higher the order of differences, the more effectively the results reflect the characteristics of high-frequency transient components in the signal and their abrupt change directions. The SOD transformation is described as follows [17]:

$$S_h(n) = \sum_{j=1}^{h+1} (-1)^{j+1} (c_j)_h Q(n-j+1) \tag{13}$$

where h represents the order of the SOD; $S_h(n)$ indicates the hth-order difference of $Q(n)$ with $Q(n)$ denoting the original signal and n signifying the instantaneous sampling point, which should satisfy the condition $n \geqslant h+1$; in addition, $(c_j)_h$ symbolizes the coefficients of the SOD transformation, and they are computed as follows.

The first and last coefficients of the SOD transformation are equal and set to 1, as:

$$(c_1)_h = (c_{h+1})_h = 1 \tag{14}$$

The second coefficient of the SOD transformation corresponds to its order, as:

$$(c_2)_h = h \tag{15}$$

The remaining coefficients of the SOD transformation can be calculated using:

$$(c_j)_h = (c_j)_{h-1} + (c_{j-1})_{h-1} \tag{16}$$

The sum of all coefficients in the SOD transformation is zero, as:

$$\sum (-1)^{j+1} (c_j)_k = 0 \tag{17}$$

In this paper, the SOD transformation is used to analyze the degree of abrupt changes in the power frequency voltage amplitude. When the voltage signal exhibits relatively uniform changes between sampling points, the differential calculation tends to approach zero, suppressing gradual variations. Conversely, when significant variations occur between sampling points, the differential calculation leads to larger changes, emphasizing abrupt variations [18]. In theory, a higher order of SOD transformation enhances the effectiveness of capturing signal fault characteristics. However, as the order increases, the expression becomes more complex, increasing computational burden and processing time. In this study, an 8th-order SOD transformation is chosen to fulfill the requirements, striking a balance between feature enhancement and computational efficiency.

IV. Single-Phase Adaptive Reclosure Strategy

A. Fault Nature Identification and Fault Extinction Time Determination

The analysis in this paper presents that during a transient fault on the transmission lines, there is a significant difference in the fault-phase fundamental frequency voltage magnitude between the secondary arc stage and the recovery voltage stage. At the same time, there is no such difference during a permanent fault. Therefore, this paper proposes a method for single-phase adaptive reclosing by detecting the significant difference in the fault-phase fundamental frequency voltage magnitude after the tripping of circuit breakers at both ends of the transmission lines.

When a single-phase ground fault occurs on the transmission lines, the circuit breaker on the faulted phase opens. Fault nature identification is delayed by 40 ms to ensure that transient overvoltage interference caused by circuit breaker tripping does not influence the accuracy of the identification criteria [19]. Within the maximum discrimination time limit $t_{\max}$, a sliding time window T_s is used to sequentially slide over the fault-phase fundamental frequency voltage magnitudes obtained through STFT and SOD transformation for cyclic detection. The criterion is as follows:

$$\left|S_{8i}(m)\right| > \varepsilon \tag{18}$$

where i denotes the sliding times of the sampling time window T_s; m represents the mth sampling point within the sliding time window T_s; and ε indicates the threshold. If a sliding window T_s satisfies (18), it is determined as a transient fault, and the fault arc extinguishes at the moment of extinction. If (18) is not satisfied for all sliding windows within the maximum discrimination time limit $t_{\max}$, it is determined as a permanent fault.

B. Single-phase Adaptive Reclosing Scheme

According to the previous analysis, the formulated adaptive reclosing scheme comprises four modules: the fault detection module, data processing module, fault nature identification module, and reclosing module. The implementation process is described in the following sections, and the scheme flow is illustrated in Fig. 5.

1) Upon detecting a single-phase fault on the wind farm transmission lines, trip the circuit breakers on both sides of the faulted phase.

2) To ensure accurate criteria despite transient overvoltage interference from tripping, start sampling the line voltage at a sampling rate of 20 kHz for a sequence $u(k)$ from 40 ms onward after the trip of the circuit breakers on the faulted phase.

3) The collected faulted-phase voltage is subjected to STFT using the window function $g(t)$ to extract the the fundamental frequency voltage magnitude $U(k)$, where k represents the instantaneous sampling point number.

4) Define the sampling time window length as w with a sliding factor of δ, constituting the sliding time window T_s. Within each sliding time window T_s, an 8th-order SOD transformation is applied to the fundamental frequency voltage magnitude $U(k)$ using the following formula:

$$S_{8i}(n)=U(n)-8U(n-1)+28U(n-2)-56U(n-3)+70U(n-4)-56U(n-5)+28U(n-6)-8U(n-7)+U(n-8) \quad (19)$$

where n ranges from 9 to N.

5) Within the maximum discrimination time limit t_{max}, fault nature identification is performed using each sliding time window T_s. If $S_{8i}(m)>\varepsilon$ within a certain time window, it is recognized as a transient fault, and the process proceeds to Step 6. Otherwise, it is recognized as a permanent fault, and the reclosing mechanism is locked, concluding the procedure.

6) The fault duration t_d is calculated based on the obtained sliding times i of the sampling window T_s, the sample point m, and the relevant circuit breaker operation times, i.e.:

$$T_d = mT_c + i \quad (20)$$

where T_c represents the time interval between two consecutive sample points, and $T_c=1/f_s$ with f_s denoting the sampling frequency.

7) At $T_h = T_d + 100$ ms, the reclosing signal is initiated to close the circuit breakers at both ends of the lines, restoring power to the system.

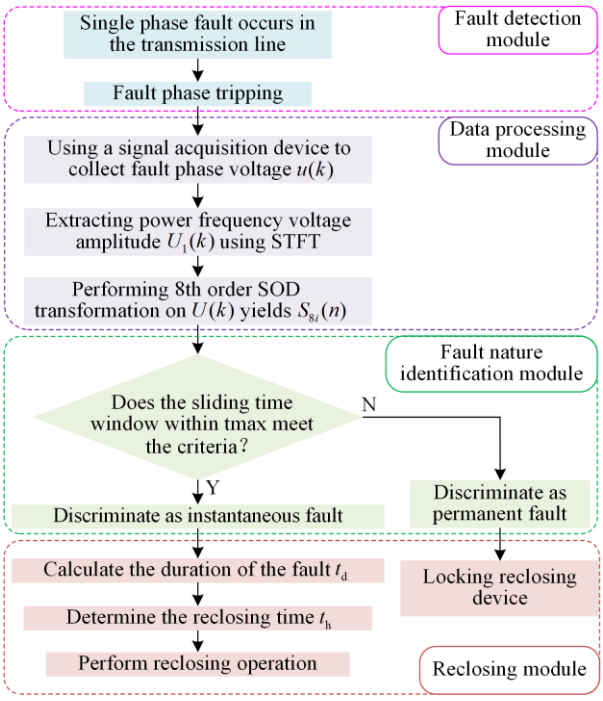

Fig. 5. Workflow of single-phase adaptive reclosing scheme.

C. Principles of Setting Fixed Values

1) Maximum Discrimination Time t_{max}

According to the operational experience of the power grid in China, the typically fixed time for automatic reclosing ranges from 0.6 s to 1.5 s [20], [21]. In this paper, a value of 0.7 s is chosen. Consequently, the circuit breaker is disconnected approximately 100 ms after the fault occurrence. Following the disappearance of the fault, time is required for the insulation recovery of the arc path. The recovery time for arc path insulation is set to 100 ms [21]. Additionally, to ensure the accuracy of the criterion for transient overvoltage interference after the circuit breaker for the faulted phase is disconnected, arc extinction detection is initiated 40 ms after the trip. Therefore, the maximum discrimination time limit is set at 460 ms. The schematic diagram of various time nodes in the reclosing process is shown in Fig. 6.

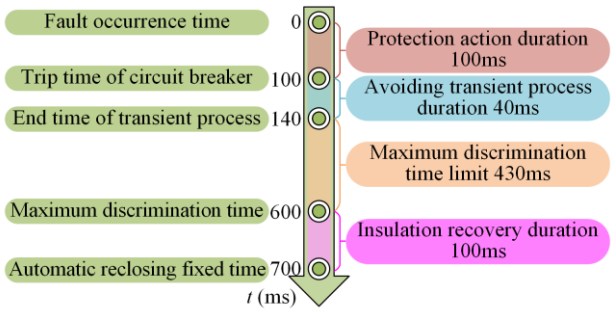

Fig. 6. Time node diagram of the reclosing process.

2) Sliding Time Window T_s

An introduced sliding time window with a width of w and a sliding factor of δ is utilized in this paper to analyze the real-time variation of fault information over time. This window performs SOD transformation on the power frequency voltage amplitude and continuously monitors whether its value satisfies the criteria for adaptive reclosing. Figure 7 depicts the schematic diagram of the sliding time window. After completing the data analysis within the first-time window, the data frame is slid forward by δ for the next round of data analysis. This process is repeated cyclically until the workflow is completed.

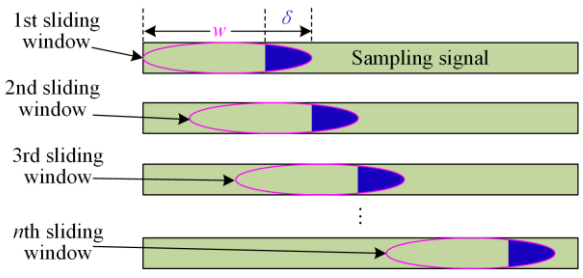

Fig. 7. Schematic diagram of the sliding time window.

In theory, reducing the sliding time window length (w) and sliding factor (δ) can improve the accuracy of

arc-extinction detection results. However, it simultaneously increases the frequency of time window movement and computational burden, which is not conducive to detecting arc-extinction moments. This paper sets w to 10 ms and δ to 1 ms to balance computational accuracy and efficiency.

3) Discrimination Threshold ε

When a permanent fault occurs on the transmission lines, the fault point persists, and the SOD-transformed fault phase power-frequency voltage amplitude remains stable and close to 0 without any sudden changes. However, for a transient fault, the SOD-transformed fault phase power-frequency voltage amplitude undergoes a noticeable sudden change around the time of fault disappearance. When the fault occurs at the line terminal, and the fault disappearance moment corresponds to the maximum discrimination time, the amplitude of the power-frequency voltage undergoes the smallest sudden change. After extensive testing and considering a certain margin, ε is set to 1 in this paper.

V. Experimental Analysis

A transmission system model for wind farms is constructed on the RTDS experimental platform to validate the practicality of the proposed single-phase adaptive reclosing scheme. The model includes 100 DFIG units, each with a rated capacity of 2 MW. The transmission lines span 100 km with a voltage rating of 220 kV, with no parallel reactor on either side of the lines. The sampling frequency is set to 20 kHz, and the RTDS experimental platform is illustrated in Fig. 8.

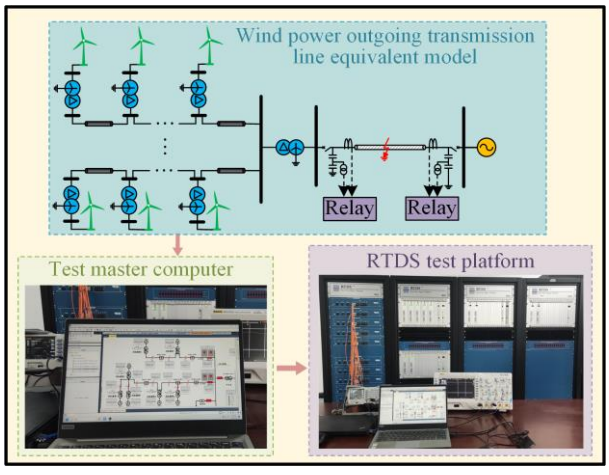

Fig. 8. RTDS experimental platform.

First, a simulation model for single-phase adaptive reclosing of wind power transmission lines is constructed on the RSCAD platform. The module encompasses steady-state operation, fault modules, circuit breakers, and external interfaces. Next, real-time digital simulation of the entire model is conducted using RTDS. The results are converted into analog signals by the GTAO board. Subsequently, a digital oscilloscope is employed to capture the analog signals, convert them into digital signals, and transmit them to the main control computer. Finally, the reclosing evaluation logic, executed on the main control computer, receives the signals, determines the fault characteristics, and issues a trip command to the circuit breaker module in RSCAD, thus completing the closed loop of the entire reclosing process.

In transmission systems of 110 kV and above, relay protection devices and measuring instruments play a crucial role, often utilizing CVTs to acquire voltage signals [22]. The equivalent model of the CVT constructed in this paper is illustrated in Fig. 9.

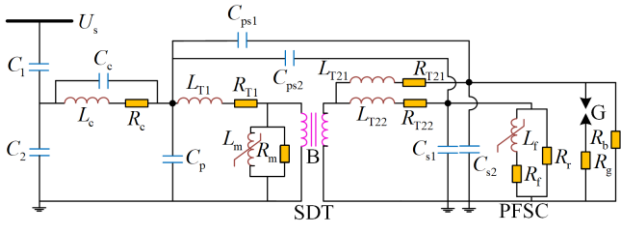

Fig. 9. Equivalent model of CVT.

In Fig. 9, the components C_1 and C_2 constitute a voltage divider circuit, reducing the primary voltage U_1 to $(C_1U_1)/(C_1+C_2)$. Within this model, the voltage across the low-voltage capacitor, C_2, is 11.6 kV. This voltage is transmitted through the compensation circuit, comprising C_c, L_c, and R_c, to the intermediate step-down transformer (SDT). Parameters C_p, C_{ps1}, C_{ps2}, C_{s1}, and C_{s2} represent the stray capacitances of the SDT's primary and secondary sides, respectively. Parameters L_{T1}, L_{T21}, L_{T22}, R_{T1}, R_{T21}, and R_{T22} denote the equivalent leakage inductances and resistances of the primary and secondary sides of the SDT, respectively. Parameters L_m and R_m account for the nonlinear inductance and resistance of the excitation branch of SDT. SDT transforms the voltage across capacitor C_2 into the secondary voltage utilized for protection and measurement. The damping circuit in this model employs a passive ferro-resonance suppression circuit (PFSC) consisting of L_f, R_f, and R_r, effectively suppressing the ferromagnetic resonance of CVT. R_b represents the load on the secondary side of CVT, while G and R_g denote protective clearances. These factors affect CVT only after overvoltage discharge breakdown and are generally not considered under normal circumstances [23].

The wind farm transmission lines introduce different natures of single-phase ground faults. The voltage signals at the protection installation are measured using the equivalent model of the CVT, as illustrated in Fig. 9. The waveforms of the CVT primary and secondary side voltages are depicted in Fig. 10. (Note: The CVT sec-

ondary side voltage mentioned here and subsequently has been normalized to the primary side.)

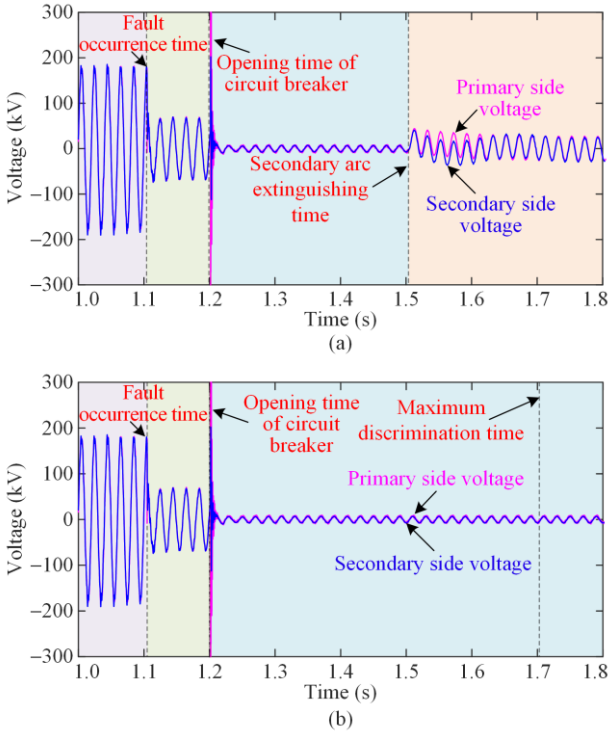

Fig. 10. Voltage waveforms on CVT primary and secondary sides. (a) Transient fault. (b) Permanent fault.

Figure 10 shows that the primary and secondary voltages are essentially coincident during the steady-state condition at the power frequency. However, distortion occurs on the CVT secondary side voltage waveform during the high-frequency transient phases. The above-mentioned adaptive reclosing scheme utilizes the power frequency voltage signal for fault nature identification. Moreover, the CVT exhibits favorable transference characteristics for this voltage signal, indicating potential practical applications in engineering.

A. Transient Fault

At $t = 1.1046$ s, a phase A metallic grounding fault occurs 30 km from the *M*-side of the wind farm transmission lines. The circuit breakers on both sides are opened 100 ms later, and the fault duration is 350 ms. Figure 11 shows the waveform of the secondary-side voltage.

Figure 11 illustrates that the voltage waveform during transient fault conditions can be divided into four stages. Stage a represents normal operation, Stage b corresponds to the primary fault arc stage from the fault occurrence until the circuit breaker opens, Stage c depicts the secondary arc stage after the circuit breaker opens, and stage d illustrates the recovery voltage stage after the secondary arc extinguishes. The voltage amplitude of the faulted phase increases significantly upon the disappearance of the fault after the circuit breaker trips. This observation is consistent with the presented theoretical analysis in this paper.

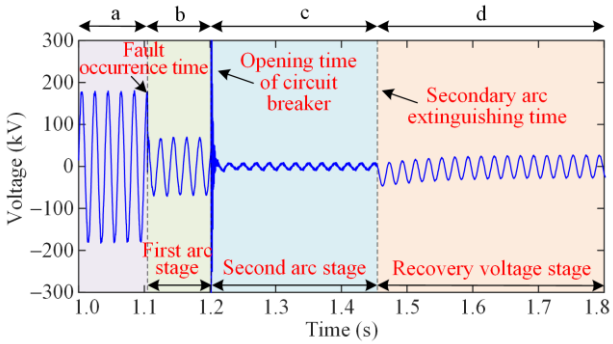

Fig. 11. Open-phase voltage waveform during transient single-phase ground fault.

According to the proposed single-phase adaptive reclosing scheme, the STFT obtains the power frequency voltage amplitude. Subsequently, the obtained power frequency voltage amplitudes undergo SOD transformation within the sliding time window T_s, as illustrated in Fig. 12. The first-time window starting the detection after the circuit breaker trip and the time window detecting the disappearance of the fault are displayed.

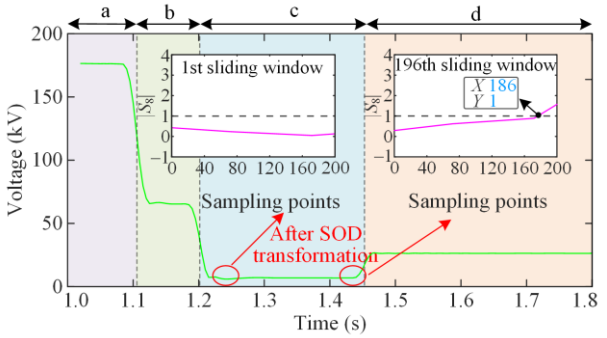

Fig. 12. Identification results of transient fault.

According to Fig. 12, the amplitude curve of the first sliding window remains constant and close to 0 during the momentary fault. At the 196th sliding window, there is a noticeable abrupt change at the 186th sampling point, indicating that the sliding time window has moved 195 times. Therefore, the fault extinguishes at 244.3 ms after the circuit breaker operation (40+195+186/20 ms =244.3 ms), while the secondary arc extinguishes at 344.3 ms after the fault occurrence. Considering the predetermined fault duration of 350 ms, the calculation error is only 5.7 ms.

B. Permanent Fault

At $t = 1.1046$ s, a phase A metallic grounding fault occurs 30 km from the *M*-side of the wind farm transmission lines. The circuit breakers on both sides are opened 100 ms later. Figure 13 shows the secondary-side voltage waveform.

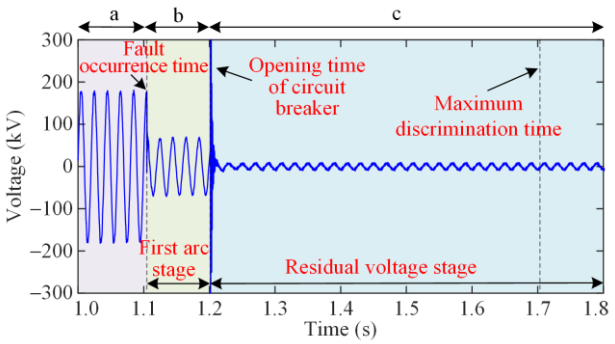

Fig. 13. Open-phase voltage waveform during permanent single-phase ground fault.

As shown in Fig. 13, stages a and b exhibit nearly identical behavior in permanent and transient faults. Stage c represents the residual voltage stage. There is no significant change in the voltage amplitude of the faulted phase after the circuit breaker opens. The amplitude approaches zero, which is consistent with the analysis presented in this paper.

The adaptive reclosing identification results are displayed in Fig. 14, showing the first-time window after tripping the circuit breaker and the time window when the detection time reaches the maximum discrimination time.

Analysis of Fig. 14 reveals that during a permanent fault on the lines, the amplitude curves for both the first and the 451st sliding windows remain constant, approaching zero. There is no apparent abrupt change after the detection within the maximum discrimination time of 460 ms. Consequently, the fault is recognized as permanent, leading to the reclosing device being locked.

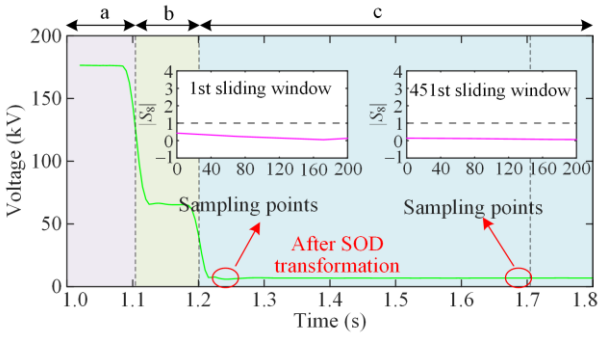

Fig. 14. Identification results of permanent fault.

C. Reliability Analysis

1) Different Fault Conditions

Considering the influence of various fault conditions on the adaptive reclosing criteria, single-phase ground faults are configured for the wind farm transmission lines under different fault locations, transitional resistances, and fault durations. The fault identification results are presented in Table I, highlighting the impact of various parameters on the adaptive reclosing scheme.

TABLE I
JUDGMENT RESULTS OF DIFFERENT FAULT CONDITIONS

Fault condition	Fault nature	Fault locations	Transition resistance (Ω)	Fault duration (ms)	Calculated fault duration (ms)	Calculated error (ms)	Discriminant results
Different fault locations	Transient	Head	0.01	350	353.65	3.65	Transient
		30 km			343.8	6.2	
		60 km			344.35	5.65	
		End			344.8	5.2	
	Permanent	Head	0.01				Permanent
		30 km					
		60 km					
		End					
Different transition resistances	Transient	30 km	0.01	350	343.8	6.2	Transient
			30		343.85	6.15	
			60		354.15	4.15	
			100		353.8	3.8	
			200		343.35	6.65	
	Permanent	30 km	0.01				Permanent
			30				
			100				
			200				
Different fault durations	Transient	30 km	0.01	200	193.35	6.65	Transient
				300	295.25	4.75	
				400	395.1	4.9	
				500	495.25	4.75	
				600	595.1	4.9	
				650			Permanent

As shown in Table I, the proposed strategy can reliably identify the nature of single-phase ground faults under various fault conditions in the transmission lines. Moreover, it can calculate the duration of transient faults with minimal computational error. In cases where the fault duration exceeds 600 ms, it is identified as a permanent fault due to the discrimination window surpassing the maximum discrimination time limit, thereby precluding reclosure.

2) Arcing Fault

An arc model is established considering the impact of arc faults on the criteria for adaptive reclosing. At $t=1.1046$ s, the different natures of phase A arcing ground faults occur 30 km from the wind farm site on the line, and, the circuit breakers are opened after 100 ms. The moment of arc extinction for transient faults is 1.3546 s. Figure 15 shows the secondary side voltage waveform of the faulty phase when an arcing fault occurs on the line.

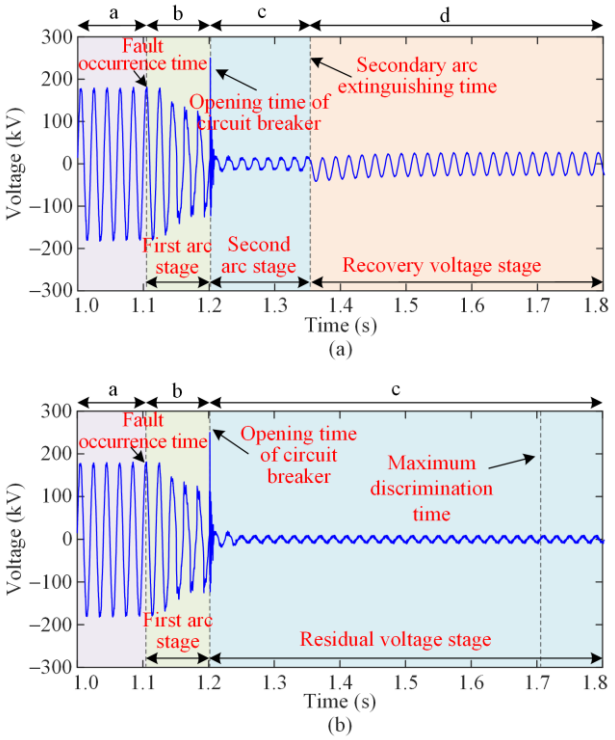

Fig. 15. Open-phase voltage waveform during arcing single-phase ground fault. (a) Transient fault. (b) Permanent fault.

The arcing fault identification results are illustrated in Fig. 16, illustrating the first window after tripping the circuit breaker and the window where the fault disappearance is detected or the maximum discrimination time is reached.

In Fig. 16(a), the amplitude curve of the first sliding window remains constant and close to 0 during the transient fault. A noticeable abrupt change occurs at the 200th sample point within the 93rd sliding window, indicating 92 movements of the sliding time window. Consequently, the fault arc extinguishes 142 ms after the circuit breaker opens (40+92+200/20 ms=142 ms), and 242 ms after the fault occurrence. In this scenario, the calculation error is only 8 ms, where the fault duration is 250 ms. In Fig. 16(b), for a permanent fault, the amplitude curves of the first and 451st sliding windows remain constant and close to 0. Following the maximum discrimination time of 430 ms, no significant abrupt change is observed, leading to the conclusion of a permanent fault without reclosing.

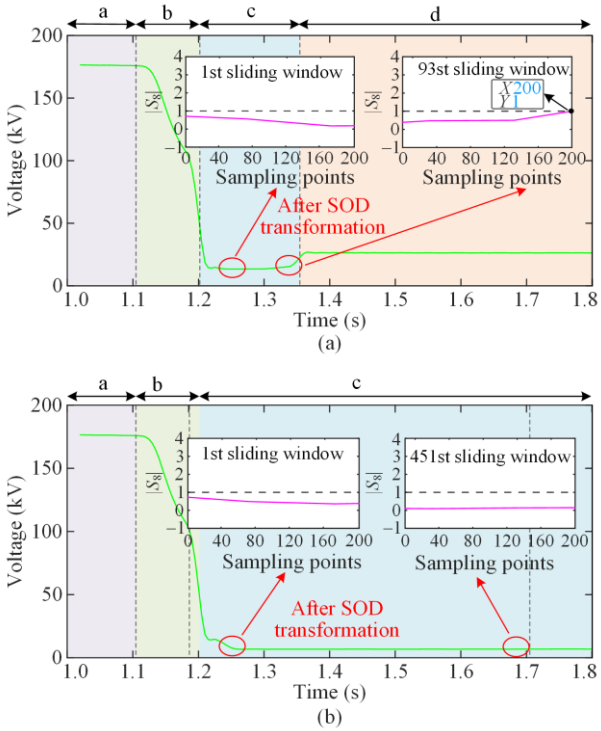

Fig. 16. Identification results of arcing single-phase ground fault. (a) Transient fault. (b) Permanent fault.

The experimental results demonstrate that the proposed method is minimally affected by factors such as transient resistance, fault location, fault duration, and arcing fault, thereby exhibiting high reliability.

D. Applicability Analysis for Traditional AC Transmission Lines

A ground fault of a different nature on phase A is placed 30 km from the system side at $t=1.1046$ s to evaluate the applicability of the proposed strategy in traditional AC transmission lines. After 100 ms, the circuit breakers on both sides of the lines are opened, with the transient fault lasting for 450 ms. Figure 17 illustrates the secondary side voltage waveforms during transient and permanent faults on traditional AC transmission lines.

The identification results of the adaptive reclosing are shown in Fig. 18. Here, the only presented results are for the cases when the first time window starts from the circuit breaker tripping and the time window where the fault disappears or the maximum discrimination time is reached.

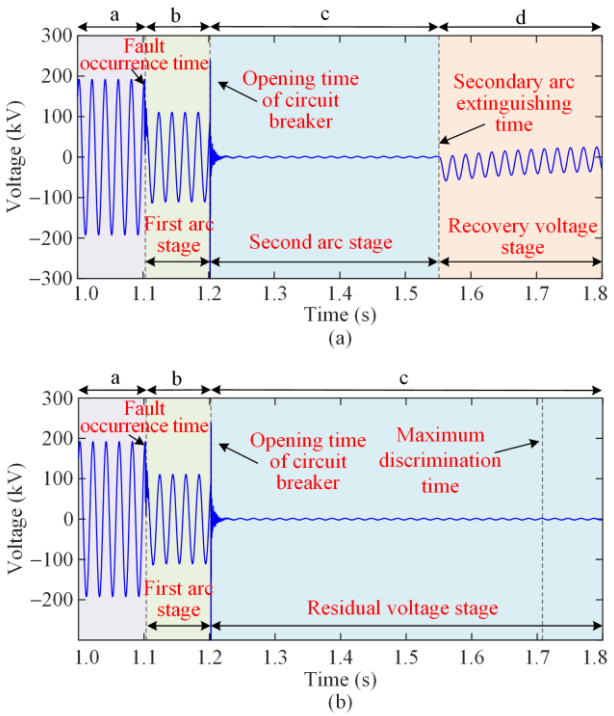

Fig. 17. Phase voltage waveform of a single-phase ground fault in traditional AC transmission lines. (a) Transient fault. (b) Permanent fault.

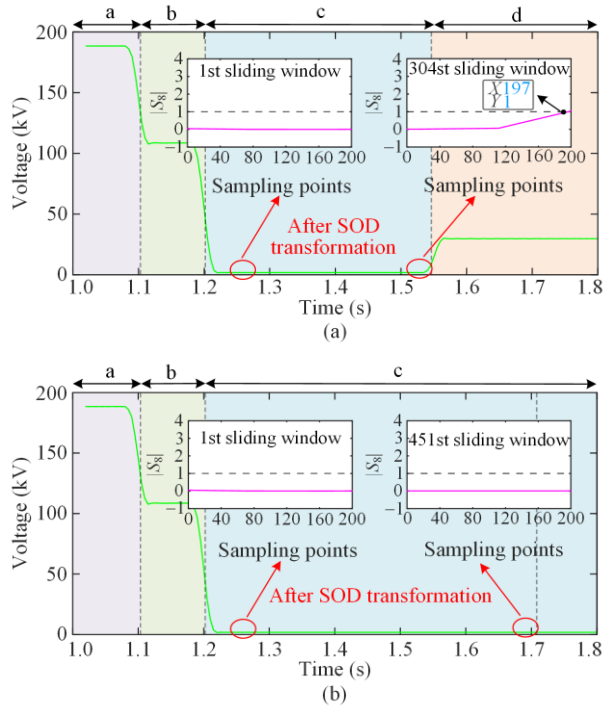

Fig. 18. Identification results of fault nature in traditional AC transmission lines. (a) Transient fault. (b) Permanent fault.

In Fig. 18(a), the amplitude curve of the first sliding window remains constant and close to 0 during the transient fault. A noticeable abrupt change occurs at the 197th sample point within the 304th sliding window, indicating 303 movements of the sliding time window. Consequently, the fault arc extinguishes 352.85 ms after the circuit breaker opens (40+303+197/20 ms=352.85 ms) and 452.85 ms after the fault occurrence. In this scenario, the calculation error is only 2.85 ms, whereas the fault duration is 450 ms. In Fig. 18(b), for the permanent fault, the amplitude curves of the first and 451st sliding windows remain constant and close to 0. No significant abrupt change is observed within the maximum discrimination time of 430 ms. Hence, it can be concluded that it is a permanent fault and reclosing is not performed.

The experimental results demonstrate that the proposed method is unaffected by power source characteristics. Therefore, this method can be applied to wind farms and traditional AC transmission lines. In both scenarios, the proposed method can accurately identify the fault characteristics, enabling adaptive reclosing and ensuring the safe and stable operation of the power system.

E. Comparison of the Effectiveness with Traditional Auto Reclosing

At $t=1.1046$ s, an arcing single-phase ground fault occurs on the A-phase, 30 km away from the wind farm side on the line. The circuit breakers on both sides are opened 100 ms later, and the fault duration is 250 ms. Fault nature identification is conducted using the proposed adaptive reclosing method, and is compared with the traditional reclosing method. Figure 19 illustrates the effects of the reclosing time for the two methods under transmission line transient fault conditions.

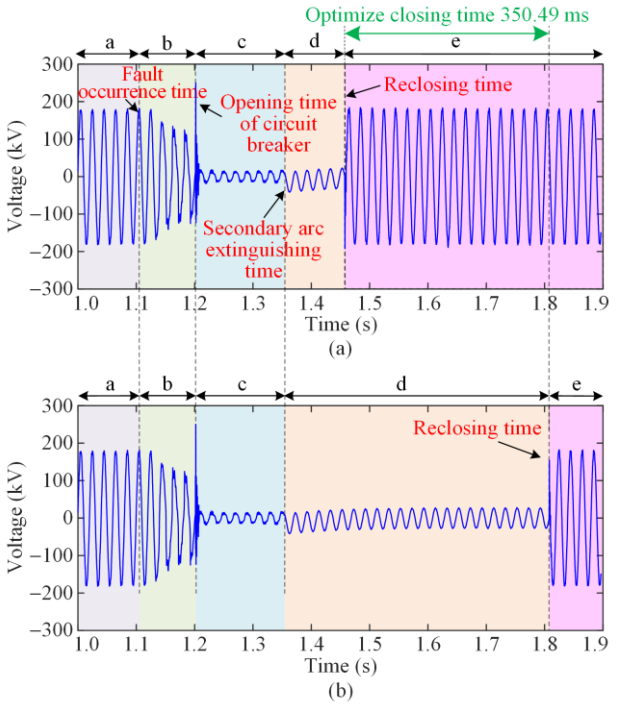

Fig. 19. Comparison of reclosing optimization time. (a) Adaptive reclosure. (b) Traditional reclosing.

Compared to the traditional automatic reclosing, the precision of the proposed method is evident in its significant improvement in reclosing time optimization under transient fault conditions, thereby greatly enhancing the power restoration speed. In the case of permanent faults, it accurately identifies and locks the reclosing device, ensuring no secondary impacts on the transmission system.

F. Comparison with Existing Adaptive Reclosing Strategies

This section compares the adaptive reclosing strategy proposed in this paper with those presented in [8] and [10]. In [8], an adaptive single-phase reclosing strategy for wind farm transmission lines is introduced based on power ratio, which can identify the moment when the fault disappears. In [10], an adaptive reclosing strategy for wind farm transmission lines based on injected current is proposed. However, this method injects a low current into the transmission lines after a fixed delay to assess the fault nature, failing to detect the moment of fault disappearance in real time. The specific comparison results between the proposed and the above two methods are shown in Table II. As seen, the proposed scheme identifies the fault nature by detecting the magnitude of the power frequency voltage on the secondary side of the coupling CVT of the healthy phase, and demonstrates a stronger ability to tolerate transition resistance. Additionally, the proposed methods in this paper and the one in [8] can identify the moment of fault disappearance. The transient fault identification results of the two schemes under different conditions are presented in Table III. It can be observed that the error in calculating the fault duration for the scheme proposed in this paper is significantly smaller than that using the method in [8]. In summary, the proposed scheme is relatively simple in principle, has good applicability, can identify the moment of fault disappearance with minimal calculation errors, and exhibits high feasibility.

TABLE II
COMPARISON RESULTS WITH EXISTING ADAPTIVE RECLOSING STRATEGIES

Scheme	The utilized signals	Application scenarios	Consideration of CVT effects	Detection of fault disappearance time	Capability of withstanding transition resistance (Ω)
[8]	Residual voltage and current	Wind farm transmission lines	No	Yes	100
[10]	Injected current	Wind farm transmission lines	No	No	50
The proposed scheme	Voltage induced by healthy phase coupling	Wind farm transmission lines	Yes	Yes	200

TABLE III
COMPARISON OF DISCRIMINATION RESULTS FOR TRANSIENT FAULTS UNDER DIFFERENT FAULT CONDITIONS WITH [8]

Scheme	Fault locations (km)	Transition resistance (Ω)	Fault duration (ms)	Calculated fault duration (ms)	Calculated error (ms)	Discriminant results
[8]	25	100	700	777	77	Transient
	50	0		734	34	Transient
	75	0		742	42	Transient
The proposed scheme	25	100	700	704.2	4.2	Transient
	50	0		694.45	5.55	Transient
	75	0		690.55	9.45	Transient

VI. CONCLUSION

This paper addresses a single-phase adaptive reclosing strategy based on detecting fundamental frequency voltage amplitude for wind farm transmission lines without parallel reactors. According to the theoretical analysis and experimental testing, several conclusions are drawn as follows.

1) The restoration voltage during a permanent fault is primarily induced by inductive coupling voltage. At the same time, it mainly composes of electromagnetic coupling voltage and capacitive coupling voltage during a transient fault. Moreover, the restoration voltage amplitude after the transient fault clearance is greater than that of a permanent fault.

2) The SOD transformation effectively suppresses the slow-changing component of the voltage amplitude while amplifies the abrupt voltage changes, significantly improving the sensitivity of fault nature identification.

3) The proposed approach utilizes the power frequency voltage amplitude for adaptive reclosing with CVTs exhibiting favorable characteristics for power frequency signals in practical engineering, making the proposed strategy promising for real-world applications.

4) Experimental results demonstrate that the reclosing strategy can reliably identify the fault nature and determine the fault clearance moment. Moreover, it exhibits excellent robustness against transient resistances,

avoids detection dead zones, and is suitable for wind farm transmission lines without parallel reactors.

ACKNOWLEDGMENT

Not applicable.

AUTHORS' CONTRIBUTIONS

Hongchun Shu: ideas, formulation of overarching research goals and aims. Cong Li: experimental design, case study, and drafting of manuscript. Yue Dai: methodology, reviewing and editing manuscript. Yutao Tang: data collection and investigation. Yiming Han: supervision, conducting a research and investigation process. All authors read and approved the final manuscript.

FUNDING

This work is supported by the National Natural Science Foundation of China (No. 52037003) and the Major Science and Technology Projects in Yunnan Province (No. 202402AG050006).

AVAILABILITY OF DATA AND MATERIALS

Not applicable.

DECLARATIONS

Competing interests: The authors declare that they have no known competing financial interests or personal relationships that could have appeared to influence the work reported in this article.

AUTHORS' INFORMATION

Hongchun Shu received his Ph.D. degree in electrical engineering from the Harbin Institute of Technology, China, in 1997. He became a professor in 1998 and completed his postdoctoral study from the Xi'an Jiao Tong University in 1999. He is currently among the famous teachers in the Yunnan Province, winning the first teaching merit of the Yunnan Province, the title of the national model teachers, the national excellent teachers, the National May 1 Labor Medal and the national excellent science and technology workers award. He presided over a total of 13 projects, including key and general projects of the National Natural Science Foundation of China, "863" projects of Yunnan province. He has more than 200 inventions as a first inventor, six books published by the state-level publishing press, 200 EI or SCI indexed papers, and one enterprise standard. He is currently a second-grade professor in China and a supervisor of Ph.D. students. His research interests include relay protection and control of power system with renewable energy, fault location of distribution power system, HVDC transmission control and protection.

Cong Li received the B.Eng. degree from the Lingnan Normal University, China in 2022. He is currently working toward the M.S. degree with the Department of Electrical Engineering, Kunming University of Science and Technology, Kunming, China. His research interest covers power transmission, transformation equipment and automation.

Yue Dai received the B.Eng. and M.S. degrees from the Kunming University of Science and Technology, China, in 2018 and 2021, respectively. She is currently working toward the Ph.D. degree with the Department of Electrical Engineering, Kunming University of Science and Technology, Kunming, China. Her research interest covers power transmission, transformation equipment and automation.

Yutao Tang received the B.Eng. degree in Shandong Jianzhu University, Jinan, China, in 2018. He is currently working toward the Ph.D. degree with the Department of Electrical Engineering, Kunming University of Science and Technology, Kunming, China. His current research interests include the relay protection and control of power system with renewable energy.

Yiming Han received the B.Eng. degree in Kunming City College, Kunming, China, in 2015, and received the Ph.D. degree from Kunming University of Science and Technology, Kunming, China in 2021. His research interests include power system protection and fault location, micro-grid automation, and renewable energy.

REFERENCES

[1] N. Verma, N. Kumar, and S. Gupta *et al*., "Review of sub-synchronous interaction in wind integrated power systems: classification, challenges, and mitigation techniques," *Protection and Control of Modern Power Systems*, vol. 8, no. 2, pp. 1-26, Apr. 2023.

[2] B. Li, D. Zheng, and B. Li *et al*., "Analysis of low voltage ride-through capability and optimal control strategy of doubly-fed wind farms under symmetrical fault," *Protection and Control of Modern Power Systems*, vol. 8, no. 2, pp. 1-15, Apr. 2023.

[3] Y. Wu, H. Gao, and T. Yuan *et al*., "Novel pilot protection for wind farm transmission lines based on Tellegen' s theorem," *Power System Protection and Control*, vol. 51, no. 6, pp. 117-126, Mar. 2023. (in Chinese)

[4] X. Liu, T. Zheng, and S. Huang *et al*., "Analysis on solution of cascade failure caused by automatic reclosing," *Power System Protection and Control*, vol. 43, no. 5, pp. 51-56, Mar. 2015. (in Chinese)

[5] B. Li, M. Li, and L. Zhao *et al*., "Impact of wind farm integration on the reclosing of high-voltage transmission lines," *Proceedings of the CSU-EPSA*, vol. 27, no. 12, pp. 23-29, Dec. 2015. (in Chinese)

[6] S. Song, C. Fu, and L. Zhang *et al*., "A coordination method of reclosing relays for wind farm grid connec-

tion line," *Automation of Electric Power Systems*, vol. 34, no. 20, pp. 77-79, 93, Oct. 2010. (in Chinese)

[7] B. Yuan, B. Zhang, and Z. Hao *et al*., "A study on auto-reclosing strategy for large-scale wind farm transmission line," in *International Conference on Power System Technology*, Chengdu, China, Oct. 2014, pp. 2827-2832.

[8] C. Xie, F. Li, and B. Wang *et al*., "An adaptive single-phase reclosing scheme based on power ratio for wind power outgoing line with shunt reactors," *Automation of Electric Power Systems*, vol. 42, no. 13, pp. 196-201, Jul. 2018. (in Chinese)

[9] H. Li, C. Xie, and W. Zhou *et al*., "Adaptive reclosing scheme for wind power outgoing line using partial-phase reclosing," *Electric Power Construction*, vol. 44, no. 5, pp. 94-107, May 2023. (in Chinese)

[10] T. Wang, G. Song, and K. S. T. Hussain, "Three-phase adaptive auto-reclosing for single outgoing line of wind farm based on active detection from STATCOM," *IEEE Transactions on Power Delivery*, vol. 35, no. 4, pp. 1918-1927, Aug. 2020.

[11] Y. Xu, Z. Lu, and W. Wang, "Study on doubly-fed wind farm transmission line reclosure time calculating," *Journal of North China Electric Power University*, vol. 44, no. 5, pp. 10-17, Sep. 2017. (in Chinese)

[12] X. Luo, C. Huang, and Y. Dai *et al*., "DC offset characteristics of recovery voltage for transient transmission line fault," *Electric Power Automation Equipment*, vol. 35, no. 1, pp. 107-111, Jan. 2015. (in Chinese)

[13] M. Jannati and J. Moshtagh, "Hardware implementation of a real-time adaptive single-phase auto-reclosure for power transmission lines," *International Transactions on Electrical Energy Systems*, vol. 30, no. 5, May 2020.

[14] M. R. D. Zadeh, I. Voloh, and M. Kanabar *et al*., "An adaptive HV transmission lines reclosing based on voltage pattern in the complex plane," in *Annual Conference for Protective Relay Engineers*, Texas, USA, Apr. 2012, pp. 85-95.

[15] J. Yang, "A new method for single-phase adaptive reclosing of ultra-high voltage AC transmission lines," M.S. thesis, the Department of Electric Engineering, Kunming university of science and technology, Kunming, China, 2015. (in Chinese)

[16] F. Zhao and R. Yang, "Voltage sag disturbance detection based on short time fourier transform," *Proceedings of the CSEE*, vol. 27, no. 10, pp. 28-34, 109, Apr. 2007. (in Chinese)

[17] H. Shu, Y. Li, and X. Tian *et al*., "Distribution network fault line selection based on correlation analysis of sequential overlapping derivative transform," *Automation of Electric Power Systems*, vol. 43, no. 6, pp. 137-144, 176, Mar. 2019. (in Chinese)

[18] H. Shu, Y. Dai, and N. An *et al*., "Fault identification method of MMC-HVDC line based on sequential overlapping derivative transform," *Transactions of China Electrotechnical Society*, vol. 36, no. 1, pp. 203-214, 226, Jan. 2021. (in Chinese)

[19] X. Luo, C. Huang, and Y. Jiang *et al*., "A voltage inner product based approach for single-phase adaptive reclosure on transmission line with shunt reactors," *Transactions of China Electrotechnical Society*, vol. 32, no. 11, pp. 17-25, Jun. 2017. (in Chinese)

[20] Z. Li, M. Zhang, and J. Wan *et al*., "Adaptive reclosure additional stability control strategy with emergency power support," *Power System Protection and Control*, vol. 51, no. 10, pp. 78-87, May 2023. (in Chinese)

[21] J. Suonan, Z. Liang, and G. Song, "Study of single-phase reclosure with adaptive secondary arc extinction," *Power System Protection and Control*, vol. 40, no. 5, pp. 37-41, Mar. 2012. (in Chinese)

[22] J. Jiang, F, Zhang, and Y. Fan *et al*., "Fault analysis of 110 kV substation PT," *Electric Power Automation Equipment*, vol. 30, no. 10, pp. 139-140, 144, Oct. 2010. (in Chinese)

[23] R. L. D. A. Reis, W. L. A. Neves, and F. V. Lopes *et al*., "Coupling capacitor voltage transformers models and impacts on electric power systems: a review," *IEEE Transactions on Power Delivery*, vol. 34, no. 5, pp. 1874-1884, Oct. 2019.